## Title

Limestone and Silica Powder Replacements for Cement: Early-Age Performance.



## Authors

Bentz, Dale
Ferraris, Chiara
Jones, Scott
et al.

## Publication Date

2017-04-01

## DOI

10.1016/j.cemconcomp.2017.01.001

Peer reviewed

**Author Manuscript**

Accepted for publication in a peer-reviewed journal

NIST National Institute of Standards and Technology • U.S. Department of Commerce

Published in final edited form as:

*Cem Concr Compos*. 2017 April ; 78: 43–56. doi:10.1016/j.cemconcomp.2017.01.001.

# Limestone and Silica Powder Replacements for Cement: Early-Age Performance

**Dale P. Bentz**[1], **Chiara F. Ferraris**[1], **Scott Z. Jones**[1], **Didier Lootens**[2], and **Franco Zunino**[1,3]

[1]National Institute of Standards and Technology, Materials and Structural Systems Division, 100 Bureau Drive, Stop 8615, Gaithersburg, MD 20899 USA

[2]Sika Technology AG- Central Research, Tueffenwies 16 CH-8048, Zurich, SWITZERLAND

[3]Pontificia Universidad Católica de Chile, School of Engineering, Department of Construction Engineering and Management, Vicuña Mackenna 4860, Macul, Santiago, CHILE

## Abstract

Developing functional concrete mixtures with less ordinary portland cement (OPC) has been one of the key objectives of the 21st century sustainability movement. While the supplies of many alternatives to OPC (such as fly ash or slag) may be limited, those of limestone and silica powders produced by crushing rocks seem virtually endless. The present study examines the chemical and physical influences of these powders on the rheology, hydration, and setting of cement-based materials via experiments and three-dimensional microstructural modeling. It is shown that both limestone and silica particle surfaces are active templates (sites) for the nucleation and growth of cement hydration products, while the limestone itself is also somewhat soluble, leading to the formation of carboaluminate hydration products. Because the filler particles are incorporated as active members of the percolated backbone that constitutes initial setting of a cement-based system, replacements of up to 50 % of the OPC by either of these powders on a volumetric basis have minimal impact on the initial setting time, and even a paste with only 5 % OPC and 95 % limestone powder by volume achieves initial set within 24 h. While their influence on setting is similar, the limestone and silica powders produce pastes with quite different rheological properties, when substituted at the same volume level. When proceeding from setting to later age strength development, one must also consider the dilution of the system due to cement removal, along with the solubility/reactivity of the filler. However, for applications where controlled (prompt) setting is more critical than developing high strengths, such as mortar tile adhesives, grouts, and renderings, significant levels of these powder replacements for cement can serve as sustainable, functional alternatives to the oft-employed 100 % OPC products.

### Keywords

Early-age hydration; heat release; limestone powder; precipitation; setting time; silica powder; sustainability

## Introduction

The reduction of cement content in concrete is one of the persistent global sustainability concerns of the 21st century [1]. Of all the ingredients in concrete (the primary ones being cement, supplementary cementitious materials, water, and coarse and fine aggregates), cement has the largest footprints when it comes to both carbon dioxide release and energy consumption. While the feasibility of achieving higher levels (greater than 50 %) of cement replacement using fly ash, a residual product from coal combustion, has been demonstrated in the laboratory and in practice [2, 3], questions remain about the stability of the supply of quality fly ash and local shortages have indeed been encountered in parts of the U.S. in recent years. Similarly, high replacement mixtures using slag have demonstrated good performance [4, 5], but the worldwide slag supply is quite limited when compared to the annual demand for concrete for new construction and repair. Consequently, all available materials options must be investigated in earnest in the quest to reduce cement content in concrete.

One material that has been used in concrete in some parts of the world for many years, but is receiving renewed interest globally, is limestone powder [3–18], typically available in the form of the calcite polymorph of calcium carbonate and with varying percentages of magnesium (carbonate). Because limestone is the major source of calcium for cement production, as well as being one of the most commonly employed aggregates, its presence is ubiquitous within the concrete industry [15]. While high purity limestone powders are produced commercially for use by the cosmetic, food, paint, paper, pharmaceutical, polymer, and concrete industries (just to name a few) [19], lower purity but more economical materials obtained as a dust-of-fracture from an aggregate crushing operation, for example, can also provide notable performance benefits in concrete [17]. Additionally, silica powder (quartz) has been investigated in several of these studies, generally comparing its performance to that of a similar-sized limestone powder [7, 9, 10 13]. For example, in comparison to a limestone powder with a median diameter of 4 μm, silica powder with a median diameter of 5 μm was found to offer equivalent early-age performance, but lower 28 d values for compressive strength, bound water, and $Ca(OH)_2$ content in both a binary blend with cement (5 % or 10 % replacement levels) and in a ternary blend containing a Class F fly ash (35 % cement replacement by mass) [9]. In contrast, for a Class C fly ash that significantly retards cement hydration at a 40 % cement replacement level by mass, while 5 % of a 4.4 μm limestone powder accelerated/amplified early-age hydration and decreased setting times markedly, 5 % of a 2.7 μm silica powder actually increased the length of the dormant period and further delayed setting times [10]. This performance difference was attributed to calcium ion availability at early ages in the two systems [10]. In a separate study of binary blends with cement, based on surface areas estimated from measured particle size distributions, the acceleration/amplification of cement hydration as quantified using isothermal calorimetry was linearly related to the supplied surface area of the limestone or quartz filler (at up to 50 % replacement levels by mass), with a greater efficiency being found for limestone than for quartz on a per unit estimated surface area basis [13].

To date, however, few studies [7, 10] have gone beyond 50:50 volumetric ratios of limestone or quartz:cement and their focus has been much more on analyzing calorimetry results

and/or compressive strengths than rheology and setting times. In the case of limestone filler, it has been suggested that its influence on setting is two-fold. First, it accelerates cement hydration. Second, with a very limited reactivity at early ages but ample surfaces that provide nucleation sites for the products of cement hydration, the virtually intact limestone particles efficiently become a part of the percolated network structure that is responsible for setting in cement-based materials [15, 20]. This is similar to a previously presented concept of using particles with a reactive shell around an inert core to optimize macro-defect-free cement-based materials [21, 22]. This paper presents an experimental and computer modeling study of the rheology, setting, and early-age hydration characteristics of binary blends of cement with either limestone or silica powder fillers with an extended range of filler volume fractions from 0 % to 95 %. For these studies, all replacements are performed on a volume for volume basis, as opposed to a mass for mass basis, due to the significant differences in specific gravities amongst the three employed powders (cement, limestone, and silica) [17].

## Materials and Methods

A locally available Type I/II ordinary Portland cement (OPC) conforming to the ASTM C150 specification [23] with a 3.7 % limestone (91.0 % $CaCO_3$) addition by mass was used in this study. The limestone powder (LS) was obtained from a commercial aggregate production plant, supplied as the dust of fracture passing through a #100 (150 μm) sieve, having an estimated $CaCO_3$ content of 98.1 % ± 0.6 % based on TGA measurements [17]. The silica powder (SA) was obtained by blending three laboratory-grade powders of similar purity to obtain a particle size distribution (PSD) similar to that measured for the LS. Oxide composition and other available characteristics of the raw materials are provided in Table 1.

PSDs of the OPC, LS, and SA were measured using laser diffraction. Isopropanol (refractive index 1.378) was used as the dispersant, and the obtained cumulative distributions are presented in Figure 1. Densities of the raw materials reported in Table 1 were measured using helium pycnometry (coefficient of variation of less than 1 %). The specific surface area of the powders was determined by the multipoint Brunauer-Emmett-Teller (BET) method, using nitrogen as the sorbent gas (typical coefficient of variation of 2 % for three replicate specimens [12]).

### Mixture proportions

Pastes were prepared and characterized with respect to initial setting time (Vicat needle according to ASTM C191 [24]) and isothermal calorimetry. The examined mixture proportions are provided in Table 2. For these mixtures, the water volume fraction (content) was maintained constant and cement was replaced by the limestone or silica powder at a 1:1 ratio on a volume basis, producing variable water-to-powder ratios (*w/p*) on a mass basis. Systems varying from 100 % OPC to 5 % OPC:95 % LS were examined. In addition, mixtures with SA were prepared, replacing 20–40–60–80 % of the cement volume. These mixtures were intended to provide a basis of comparison between limestone and silica powder performance.

For these studies, powders were first pre-blended for 30 min using a laboratory shaker-mixer that simultaneously rolls and tumbles the (mixing) container. Following preparation of the paste in a temperature-controlled high shear blender according to ASTM C1738 [24], a rubber conical frustum mold was filled for the measurement of initial setting time and about 5 g of paste were placed in a sealed glass vial for isothermal calorimetry measurements. Heat of hydration was monitored to 7 d at 23 °C, beginning approximately 30 min after the water contacted the cement. Thus, the initial exothermic dissolution heat peak was not included in the data obtained in this study. Setting was monitored using an automatic (Vicat) instrument that spun and relocated the specimen to make needle penetration measurements in fresh locations every 10 min, starting after a user-selected delay. According to the ASTM C191 test method [25], the single laboratory precision for initial time of setting (taken as the time when a penetration of 25 mm is first achieved) is 12 min. For calorimetry measurements, the average absolute difference between replicate specimens was previously measured to be $2.4 \times 10^{-5}$ W/g (cement), for measurements conducted between 1 h and 7 d after mixing [26].

Separate paste mixtures were prepared for the rheology measurements, using the same mixing procedure as that used to prepare pastes for isothermal calorimetry and setting time measurements. Mixtures with 40 % limestone or silica volume replacements were studied, in addition to the 100 % OPC control, using the proportions shown in Table 2. The temperature of the water cooling unit attached to the high shear blender was set to 14 °C, in order to achieve a final mixture temperature close to 23 °C. After mixing, specimens were stored in a hermetically sealed vacuum bottle. For these same mixtures, the maximum packing fraction of the solid particles was estimated based on centrifuge measurements of “extractable” water [17]. For the OPC, LS, and SA mixtures, maximum packing fractions of 61.1 %, 60.2 %, and 63.1 %, respectively, were measured. As the solids concentration in a mixture approaches its corresponding maximum packing fraction, rheological properties usually diverge (increase dramatically) due to jamming, etc. For comparison, the initial solids concentration of each mixture in Table 2 is 44.2 %.

Rheological tests were performed 15 min after mixing to assess the initial consistency and yield stress of the mixtures. Evolution of the shear stress was evaluated by applying shear rates from 100 $s^{-1}$ to 0.1 $s^{-1}$. For this measurement, a 40.6 mm diameter and 47.9 mm length spiral device was selected to avoid slippage and thereby provide a better estimate of the initial rheological properties. The container was 43 mm in diameter and 96 mm deep. Thus, the gap at the circumference was 1.2 mm. The geometry was calibrated using NIST Standard Reference Material (SRM) 2492 [27] to convert the torque and rotational speed measured to shear stress and shear rate. The yield stress and the consistency factor (similar to a plastic viscosity) are determined by a power law fit according to the Herschel-Bulkley model (Eq. 1):

$$\tau = \tau_0 + \mu \dot{\gamma}^n \quad (1)$$

where $\tau$ is the applied shear stress (Pa), $\tau_0$ is the yield stress (Pa), $\mu$ is the consistency factor (Pa·$s^{-n}$), $\dot{\gamma}$ is the shear rate ($s^{-1}$), and $n$ is the flow (power law) index.

Following the initial variable shear rate measurements, stress growth measurements were conducted, starting at 30 min, and repeated approximately every 10 min up to 3 h after contact of water and cementitious materials. The stress growth test is characterized by the material being sheared at a very low shear rate (0.1 $s^{-1}$ herein). A parallel plate device with a set of 35 mm diameter serrated test plates was used to conduct this test. The gap was set to 0.600 mm ± 0.001 mm and the temperature was controlled at 23 °C ± 0.2 °C. Using a syringe, approximately 1.3 mL of fresh paste was placed on the lower plate for each measurement. The stress was recorded for a period of 400 s. For this test protocol, the stress-time curve has three well defined stages, and the maximum peak value is used as a good approximation of the static yield stress [26, 28].

## Computer Modelling

CEMHYD3D version 3.0 [29] with either an inert or limestone (reactive) filler was employed to simulate the paste experiments. The model has been employed previously to simulate the influence of limestone fillers on hydration and microstructure development [20, 30]. In the model, limestone particle surfaces are available for the precipitation and growth of calcium silicate hydrate gel (C-S-H) hydration product and the limestone particles are considered to be part of a (connected) skeleton that produces setting. Additionally, the limestone is mildly soluble, reacting with the aluminate phases present in the cement to produce a mono-carboaluminate hydration product. As has been indicated by X-ray diffraction results in real pastes [9, 14], mono-carboaluminate formation is typically preceded by the formation of a hemi-carbonate hydration product(s), but this pre-cursor product is not included in the current CEMHYD3D simulations.

The PSD of the simulated cement and cement/filler blends is provided in Figure 1. For convenience, the number of each diameter particle was fixed to be a multiple of five, so that splits into 20:80, 40:60, 60:40, and 80:20 volumetric blends were readily achieved. For each blended paste, the particles with a diameter larger than 1 μm were placed from largest to smallest at random locations in the 3-D computational volume, with no effort being made to either disperse or flocculate them. The particles 1 μm (1 voxel) in diameter were then placed following the phase distribution amongst the larger particles and just prior to beginning the hydration simulation, so that their phases could be assigned in such a manner as to match the desired phase fractions of the cement (and limestone or inert filler) [29]. Phase volume fractions for the four major clinker phases were selected to match the data provided in Table 1, with the assumption that the phase surface area fractions were equal to their volume fractions. It was further assumed that the calcium sulfate was present as a 50:50 mixture of dihydrate and hemihydrate (designated as half-hemi in the graphs to follow). Representative two-dimensional slices from the 3-D starting microstructures following the placement of the 1 μm particles are shown in Figure 2, along with a few examples of the microstructures produced by 1000 cycles (420 h) of hydration.

Needle penetration measurements of setting were related to the percolation of total solids in the model 3-D microstructures and simulated heat flow and heat release results were compared directly to their experimental counterparts. The model factor to convert from hydration cycles to time was calibrated based on the measured calorimetry results for the

100 % OPC system and then maintained at that determined value (0.00042 h/cycle$^2$) for all of the simulations for the various blended pastes. While the model results could have been adjusted to exactly match the calorimetry results for each system being investigated, the use of a single calibration factor was deemed adequate for the purposes of the present study.

## Results

### Rheology

Measured shear stress versus shear rate and yield stress versus time are shown in Figures 3 and 4, respectively. In Figure 3, the shear stress versus shear rate correlations are not linear, particularly for shear rates below 10 $s^{-1}$. This has been previously observed and suggests a dependence of the slope (consistency or viscosity) with the shear rate [28]. Therefore, the Herschel-Bulkley model (Eq 1) is taken instead of a Bingham (linear, $n = 1$) plot. The fitting parameters of the equations for each curve are summarized in Table 3. The flow index $n$ has been kept constant for a better comparison of the yield stress and consistency factors. Both yield stress and consistency factors are relatively constant with time for both LS and SA substitution and change slightly more for the pure OPC. The yield stress of the paste prepared with 40 % LS substitution is about half of that obtained with either the OPC or the SA.

Considering that the PSDs and specific surface areas of the LS and SA powders are nominally similar (Figure 1 and Table 1, respectively) and that replacements were made on a volumetric basis (thus, initial water volume fraction was kept constant), their influence on early age rheology is significantly different. While SA maintains a similar initial flow behavior compared to the 100 % OPC mixture, LS provides meaningful enhancements in the mixture flowability, as evidenced by its lower yield stress (Figure 4 and $\tau_o$ in Table 3). This occurs even though the measured maximum packing fraction for the LS mixture is less than that of the OPC and SA systems. Furthermore, as this enhancement is not seen with the SA mixtures, the observed effect cannot be attributed to OPC dilution alone, suggesting that limestone particles may be providing additional lubrication to the cement paste. The calcite (main constituent of the LS powder used in this study) cleavage plane ($10\bar{1}4$) contains $Ca^{+2}$ and $CO_3^{-2}$ ions, making the surface neutral, and it is always terminated by oxygen atoms [31, 32], as seen in Figure 5. In aqueous solution, hydroxyl groups ($OH^-$) localize over the calcite ($Ca^{+2}$) surface [32], which may provide a means of inter-particle electrostatic repulsion and thus, enhance the flowability of the suspension (much like a polycarboxylate-based high range water reducer absorbs on the cement particle surfaces and prevents/reduces cement particle to cement particle flocculation). In fact, when used in self-consolidating concretes (SCCs), limestone powder is sometimes referred to as a mineral plasticizer.

Figure 4 shows that the yield stress increases monotonically up to the time where a rapid increase in the slope appears. It should be noted that the acceleration of the yield stress increase corresponds to the loss of slump measured classically with a slump test. Two linear fits of both stages were added in the graphic of Figure 4 to permit determination of their intersection, corresponding to the beginning of the slump loss of the pastes. The yield stress measured with the rheometer is several orders of magnitudes smaller than the ones determined by Vicat tests for the same mixtures (as subsequently shown in Figures 8 and 9)

[33]. The rheometer has a higher sensitivity than a Vicat apparatus, which allows detection of small changes in yield stress that the Vicat apparatus doesn't measure [28]. However, both methods rank the setting (times) of the mixtures in the same order [26, 33].

## Isothermal calorimetry

The isothermal calorimetry results for the pastes with LS and SA replacement for cement are provided in Figures 6 and 7, respectively. The heat flow results are normalized per g of OPC and are quite similar to some presented previously for LS and SA binary blend systems [10, 13], while the cumulative heat release results are normalized per unit volume of water in the initial mix, as this quantity has been shown to be highly indicative of strength development [10, 35]. In Figure 6, the LS is seen to both accelerate and amplify the cement hydration reactions, particularly amplifying those usually attributed to a renewed reactivity of the aluminate phases (upon calcium sulfate depletion [36]) for LS contents of 80 % and higher. The SA (Figure 7) also provides acceleration and amplification of the early-age hydration (but slightly less so than the LS), and does affect the aluminate reactions, especially when employed at the 80 % level.

While carboaluminates, as opposed to sulfoaluminates, are known to form when LS is present [8, 14, 37], aluminate reaction enhancement by the silica is more surprising. For both fillers, some of this enhancement in the 80 % (and higher) replacement level mixtures may be due to the surplus of surface area available for initial hydrate precipitation allowing for a more vigorous (renewed) reaction of the less covered aluminate phases within the cement (multi-phase particles), once the sulfates are depleted. While cement dilution dominates the cumulative heat release (translated to strength) response at 1 d and beyond, for systems with up to 50 % LS (Figure 6) or 40 % SA (Figure 7), the normalized cumulative heat release response is fairly independent of filler level during about the first 12 h of hydration, corresponding to a cumulative heat release of up to about 150 J/mL water. As is shown in the results that follow, this time (or heat release) period encompasses that required for achieving initial set in these same mixtures.

## Setting time

Measured setting times for the studied paste mixtures are presented in Figures 8 and 9 for the mixtures with LS and SA, respectively. At all OPC-by-filler replacement levels, the powders provide extra surface for the heterogeneous nucleation of cement hydration products [7, 13, 15]. For replacement levels of up to about 50 %, hydration is effectively accelerated to an extent that is able to offset the cement dilution effect, the latter dominating at higher replacement levels (above 50 %). This can be seen in the 10 %, 20 %, and 40 % LS mixtures which exhibit a slightly shorter initial setting time as compared to the 5 % LS mixture in Figure 8 (also see the inset in Figure 10). On the other hand, beyond about 50 % LS volume replacement, the dilution effect dominates over the enhanced hydration, and the setting times increase with filler content, in inverse proportion to cement volume fraction (Figure 10). In comparing the results with the SA and LS fillers in Figure 9, it can be seen that the setting times of the pastes prepared with SA are slightly delayed with respect to those provided by LS, even though the measured surface area of the SA on a unit volume basis is 20 % larger than that of the LS (Table 1). Two possible contributors to this result are

the formation of some carboaluminates in the LS pastes and a possibly inherently higher efficiency of the LS surfaces over those of the SA with respect to the nucleation and growth of cement hydration products, mainly C-S-H [13].

Figure 11 shows the heat release achieved at the initial time of set plotted vs. the OPC replacement level. For both fillers, the amount of heat release (hydration) required to produce set is fairly constant at 40 J/mL water ± 10 J/mL water. Since the volume fraction of particles (and water) is constant across all of the mixtures, this implies that it is taking the same amount of hydration to connect these particles into a percolated (set) structure regardless of the ratio of filler to cement particles, as will be explored in more detail in the computer modeling results to follow. In each case in Figure 11, the mixture with SA, although requiring a longer time to achieve initial set (Figure 9), achieved setting at a lower cumulative heat release than the corresponding mixture prepared with LS.

## Computer Modeling Results

The computer modeling results for setting and calorimetry are provided in Figures 12 and 13, respectively. In Figure 12, the fraction of connected solids from CEMHYD3D is directly compared to the needle penetration readings [38], with 37 % connected solids approximately corresponding to the initial setting condition. In Figure 13, for clarity, only the calorimetry results obtained for the LS mixtures are shown, and the model results for cumulative heat release were reset to zero at the time corresponding to when experimental calorimetry data was first obtained for each mixture (typically at about 0.7 h). As mentioned previously, the CEMHYD3D results for the 100 % OPC mixture were calibrated to the experimental results and the so-obtained calibration (time conversion) factor was maintained constant for all of the mixtures with fillers. The model is being applied to verify the conjecture that the filler particles, in addition to accelerating the hydration reactions, are active participants in the bridge-building process that leads to setting and subsequent strength development. Since the model provides a complete three-dimensional description of the developing microstructure, simulations can be executed both where the filler particles are considered to be part of this percolated structure and where they are considered as being isolated from any developing 3-D structure spanning the computational volume.

In comparing the setting time results in Figure 12, it is important that the model has adequately captured the hydration kinetics. In Figure 13, it is observed that each of the model systems with LS have achieved the same cumulative heat release as their experimental counterpart at an age of about 8 h, although the LS simulations often show a slightly greater acceleration than their experimental counterparts at earlier ages. To further verify this approach, Figure 14 provides a direct comparison of setting to cumulative heat release (bypassing time as an intermediate variable) for the 40:60 OPC:LS mixture and a good agreement is indeed observed between experimental and model LS results. Similarly, in Figure 12, in every case, a good agreement is seen between experimental and CEMHYD3D results for setting plotted vs. time, when the (LS) filler particles are included as part of the percolated structure comprising setting. When a totally inert filler particle is used, hydration reactions are delayed due to cement dilution, with no counterbalancing acceleration being provided by the filler (surfaces). This would naturally lead to a delay in

setting, but even when the kinetics are adjusted in the 40:60 OPC:inert filler mixture to match the experimental results (Figure 13), the predicted setting (Figure 12) is still greatly delayed in comparison to that measured experimentally. This can also be directly seen in Figure 14 where the inert filler simulation results lag significantly behind those of the experimental data when both are plotted against cumulative heat release. In a separate simulation for the 60:40 OPC:LS mixture, the LS was allowed to accelerate the cement hydration, but not participate in the percolated structure development. Once again, the setting response predicted in this case was significantly delayed with respect to that observed experimentally. Together, these simulations support the hypothesis that the filler particles must be active participants in the percolated structure that leads to setting in these binary blends (essentially functioning as inert cores with (re)active surfaces [21, 22]). Therefore, one would expect that in the mixtures investigated in this study, all with the same volume fractions of water and initial solids particles, the same amount of hydration (per unit volume of water) would be required to produce initial setting, i.e., the experimental result first shown in Figure 11.

## Implications for Strength

Assuming that cumulative heat release normalized per unit volume of water is proportional to strength [35], further analysis of the heat release results with the different filler replacement levels for cement can be used to infer filler efficiency with respect to strength enhancement. The 7 d cumulative heat release for all of the systems with either LS or SA filler replacing cement is less than that of the 100 % OPC paste due to the dilution of the cement content, but some benefit above the value based on dilution alone is observed due to the filler's acceleration of the early-age cement hydration reactions. In this regard, the plots in Figure 15 illustrate the extra heat release (strength) that was measured in mixtures with LS or SA, above the value that would be expected by only considering dilution of the cement in each mixture. Similar results using quartz (silica) fillers have been obtained by Cyr *et al.* [7], using degree of cement hydration as the dependent variable as opposed to heat release. While all of the mixtures contribute additional heat above that expected based on simple cement dilution, due to the filler acceleration of hydration, maximum efficiency in terms of promoting cement reactions is achieved at a 40 % filler replacement for cement (60 % OPC volume fraction in Figure 15) for both LS and SA, for the 24 h and even more so for the 7 d measurements. For their quartz fillers at replacement rates of 10 %, 25 %, 50 %, and 75 %, Cyr *et al.* [7] observed a maximum in excess of hydrated cement at the 25 % replacement level at ages of 24 h and 48 h, in general agreement with the trends obtained in this study. At later ages, as nearly all of the cement will be consumed regardless of the replacement level, the data in Figure 15 should approach the dilution effect line. Still, the systems with limestone replacement may exhibit some strength enhancement above the level expected from only dilution, perhaps due to the formation of carboaluminates that are stiffer than conventional cement hydration products [9, 17, 39]. Considering the gain in heat release relative to the potential heat release of the diluted OPC, it can be observed that this magnitude always increases, both for the LS and the SA systems (Figure 15c). This is consistent with isothermal calorimetry results, where it was seen that the addition of LS or SA accelerated OPC hydration even at the highest replacement levels (Figures 6 and 7). Furthermore, this relative increase in heat release appears to be linear for all LS systems at

24 h and up to 40 % LS (60 % OPC volume fraction) replacement at 168 h, in good agreement with the maximum efficiency replacement observed considering the absolute heat gain of the mixtures with LS and SA.

## Conclusions

The ability of both limestone and silica powders to accelerate early-age hydration and reduce/maintain initial setting times has been demonstrated. When used as partial replacements for cement, these fillers provide ample surfaces to serve as templates for the growth of cement hydration products and their relatively inert cores become incorporated as part of the three-dimensional percolated backbone that provides setting, rigidity, and strength to these materials. The precipitation-friendly surfaces of the fillers reduce the amount of hydration product precipitation occurring initially on the cement particles, so that the renewed reactivity of (unexposed) aluminates, etc., typically observed as a second heat flow peak or a shoulder on the primary hydration peak, is enhanced, particularly for cement replacement levels of 80 % and higher. While the limestone powder is slightly more efficient at accelerating hydration than the silica on a per unit surface area basis, it provides further benefits in rheological properties by reducing the yield stress and lowering the consistency factor, when used to replace cement on a one-to-one volume basis. Due to their acceleration of cement hydration, replacement levels of up to 40 % of these fillers for cement have minimal impact on initial setting times, suggesting that these sustainable binary blends may be particularly attractive in applications where controlled setting is more important than development of high strengths, such as mortar tile adhesives, other grouts, and renderings for building facades.

## Acknowledgments

The authors gratefully acknowledge Mr. Max Peltz (NIST) for performing the PSD, helium pycnometry, and BET surface area measurements on the powders used in this study. The provision of materials by Carmeuse and the Lehigh Cement Company are gratefully acknowledged. The authors also acknowledge Pontificia Universidad Católica de Chile and the Chilean Ministry of Education (MINEDUC) through their agreement PUC1202 for funding Franco Zunino’s internship at NIST.

## References

1. Schneider M, Romer M, Tschudin M, Bolio H. Sustainable Cement Production – Present and Future. Cement and Concrete Research. 2011; 41(7):642–650.
2. Bentz, DP., Ferraris, CF., Snyder, KA. Best Practices Guide for High-Volume Fly Ash Concretes: Assuring Properties and Performance. U.S. Department of Commerce; Sep. 2013 NIST Technical Note 1812
3. Howard IL, Shannon J, Cost VT, Stovall M. Davis Wade Stadium Expansion and Renovation: Performance of Concrete with Portland-Limestone Cement, Fly Ash, and Slag Cement. Journal of Materials in Civil Engineering. 2015; 27(12)
4. Menéndez G, Bonavetti V, Irassar EF. Strength Development of Ternary Blended Cement with Limestone Filler and Blast-Furnace Slag. Cement and Concrete Composites. 2003; 25(1):61–67.
5. Shannon J, Howard IL, Cost VT. Potential of Portland-Limestone Cement to Improve Performance of Concrete Made with High Slag Cement and Fly Ash Replacement Rates. ASTM Journal of Testing and Evaluation. 2017; 45(3):1–17.
6. Bonavetti V, Donza H, Menéndez G, Cabrera O, Irassar EG. Limestone Filler Cement in Low *w/c* Concrete: A Rational Use of Energy. Cement and Concrete Research. 2003; 33:865–871.

7. Cyr M, Lawrence P, Ringot E. Mineral Admixtures in Mortars: Quantification of the Physical Effects of Inert Materials on Short-Term Hydration. Cement and Concrete Research. 2005; 35:719–730.
8. Lothenbach B, Le Saout G, Galluci E, Scrivener K. Influence of Limestone on the Hydration of Portland Cements. Cement and Concrete Research. 2008; 38:848–860.
9. De Weerdt K, Ben Haha M, Le Saout G, Kjellsen KO, Justnes H, Lothenbach B. Hydration Mechanisms of Ternary Portland Cements Containing Limestone Powder. Cement and Concrete Research. 2011; 41:279–291.
10. Bentz DP, Sato T, De la Varga I, Weiss WJ. Fine Limestone Additions to Regulate Setting in High Volume Fly Ash Mixtures. Cement and Concrete Composites. 2012; 34(1):11–17.
11. Chowaniec, O. Ph D Thesis. École Polytechnique Fédérale de Lausanne; 2012. Limestone Addition in Cement.
12. Gurney L, Bentz DP, Sato T, Weiss WJ. Reducing Set Retardation in High Volume Fly Ash Mixtures with the Use of Limestone: Improving Constructability for Sustainability. Journal of the Transportation Research Board. 2012; (2290):139–146. Transportation Research Record. Concrete Materials 2012.
13. Oey T, Kumar A, Bullard JW, Neithalath N, Sant G. The Filler Effect: The Influence of Filler Content and Surface Area on Cementitious Reaction Rates. Journal of the American Ceramic Society. 2013; 96(6):1978–1990.
14. Zajac M, Rossberg A, Le Saout G, Lothenbach B. Influence of Limestone and Anhydrite on the Hydration of Portland Cements. Cement and Concrete Composites. 2014; 46:99–108.
15. Bentz DP, Ardani A, Barrett T, Jones SZ, Lootens D, Peltz MA, Sato T, Stutzman PE, Tanesi J, Weiss WJ. Multi-Scale Investigation of the Performance of Limestone in Concrete. Construction and Building Materials. 2015; 75:1–10.
16. Nkinamubanzi, PC., Talbot, C. Optimization of the Use of Ground Limestone in Concrete; Proceedings of the Thirteenth International Conference on Recent Advances in Concrete Technology and Sustainability Issues; Ottawa, Canada. July 2015;
17. Bentz, DP., Jones, SZ., Lootens, D. Minimizing Paste Content in Concrete Using Limestone Powders – Demonstration Mixtures. U.S. Department of Commerce; Jan. 2016 NIST Technical Note 1906
18. Antoni M, Rossen J, Martirena F, Scrivener K. Cement Substitution by a Combination of Metakaolin and Limestone. Cement and Concrete Research. 2012; 42(12):1579–1589.
19. Longcliffe Calcium Carbonates. The Processing and Major Uses of Limestone. p. 4http://www.longcliffe.co.uk/pdf/The Processing and Major Uses of Limestone.pdf, accessed May 2016
20. Bentz DP. Activation Energies of High-Volume Fly Ash Ternary Blends: Hydration and Setting. Cement and Concrete Composites. 2014; 53:214–223.
21. Desai P, Lewis JA, Bentz DP. Unreacted Cement Content in Macro-Defect-Free Composites: Impact on Processing-Structure-Property Relations. Journal of Materials Science. 1994; 29(4): 6445–6452.
22. Desai PG, Xu Z, Lewis JA. Synthesis and Properties of $CaAl_2O_4$-Coated $Al_2O_3$ Microcomposite Powders. Journal of the American Ceramic Society. 1995; 78(11):2881–2888.
23. ASTM International. ASTM C150/C150M-12, Standard Specification for Portland Cement. ASTM International; West Conshohocken, PA: 2012. p. 9
24. ASTM International. ASTM C1738/C1738M-14, Standard Practice for High-Shear Mixing of Hydraulic Cement Pastes. ASTM International; West Conshohocken, PA: 2014. p. 3
25. ASTM International. ASTM C191-13, Standard Test Methods for Time of Setting of Hydraulic Cement by Vicat Needle. ASTM International; West Conshohocken, PA: 2013. p. 8
26. Bentz DP, Ferraris CF. Rheology and Setting of High Volume Fly Ash Mixtures. Cement and Concrete Composites. 2010; 32(4):265–270.
27. Olivas, A., Ferraris, CF., Guthrie, WF., Toman, B. Re-Certification of SRM 2492: Bingham Paste Mixture for Rheological Measurements. Aug. 2015 NIST SP-260-182certificate available at: https://www-s.nist.gov/srmors/certificates/2492.pdf?CFID=42133344&CFTOKEN=1344caf90f900336-ACE05E97-9317-9ED5-20F7E8244F82C739

28. Amziane S, Ferraris CF. Cementitious Paste Setting Using Rheological and Pressure Measurements. ACI Materials Journal. 2007; 104(2):137–145.
29. Bentz, DP. CEMHYD3D: A Three-Dimensional Cement Hydration and Microstructure Development Modeling Package. Version 3.0. Technology Administration, U.S. Department of Commerce; Jun. 2005 NISTIR 7232software available for free download at: ftp://ftp.nist.gov/pub/bfrl/bentz/CEMHYD3D/version30/
30. Bentz DP. Modeling the Influence of Limestone Filler on Cement Hydration Using CEMHYD3D. Cement and Concrete Composites. 2006; 28(2):124–129.
31. de Leeuw NH, Parker SC. Surface Structure and Morphology of Calcium Carbonate Polymorphs Calcite, Aragonite, and Vaterite: An Atomistic Approach. Journal of Chemical Physics B. 1998; 102:2914–2922.
32. Sekkal W, Zaoui A. Nanoscale Analysis of the Morphology and Surface Stability of Calcium Carbonate Polymorphs. Scientific Reports. 2013; 3:1587, 1–10. [PubMed: 23545842]
33. Lootens D, Jousset P, Martinie L, Roussel N, Flatt RJ. Yield Stress during Setting of Cement Pastes from Penetration Tests. Cement and Concrete Research. 2009; 39:401–408.
34. Momma K, Izumi F. VESTA 3 for Three-Dimensional Visualization of Crystal, Volumetric and Morphology data. Journal of Applied Crystallography. 2011; 44:1272–1276.
35. Bentz DP, Barrett T, De la Varga I, Weiss WJ. Relating Compressive Strength to Heat Release in Mortars. Advances in Civil Engineering Materials. Sep.2012 1(1):14.
36. Taylor, HFW. Cement Chemistry. 2nd. Thomas Telford; London: 1997.
37. Bonavetti VL, Rahhal VF, Irassar EF. Studies on the Carboaluminate Formation in Limestone Filler-Blended Cements. Cement and Concrete Research. 2001; 31:853–859.
38. Bentz D. Cement Hydration: Building Bridges and Dams at the Microstructure Level. Materials and Structures. 2007; 40(4):397–404.
39. Moon J, Oh JE, Balonis M, Glasser FP, Clark SM, Monteiro PJM. High Pressure Study of Low Compressibility Tetracalcium Aluminum Carbonate Hydrates $3CaO{\cdot}Al_2O_3{\cdot}CaCO_3{\cdot}11H_2O$. Cement and Concrete Research. 2012; 42:105–110.

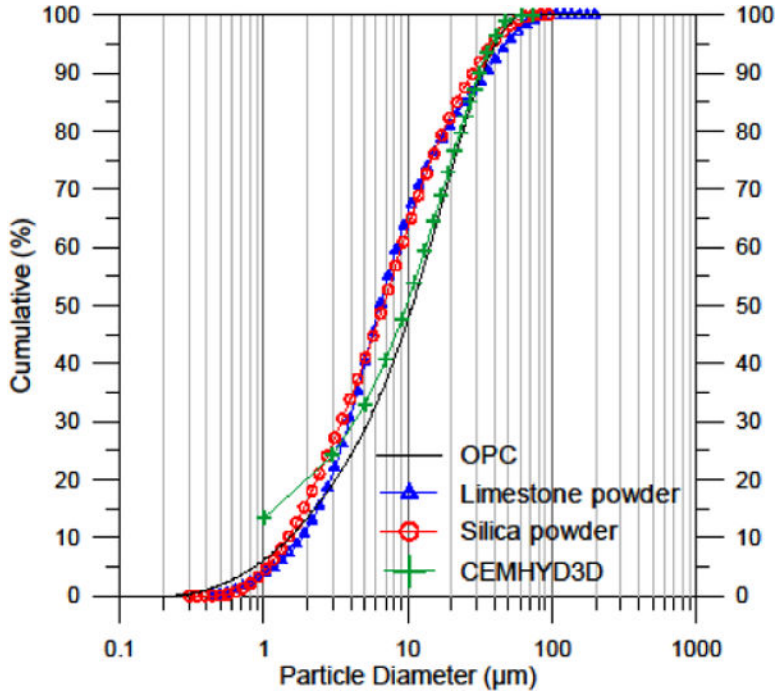


**Figure 1.**

PSDs of the raw materials determined using laser diffraction. The displayed results are the average of six individual measurements and error bars (one standard deviation) would fall within the size of the symbols on the plot. For CEMHYD3D, a single distribution was used to model both the OPC and blended cements.

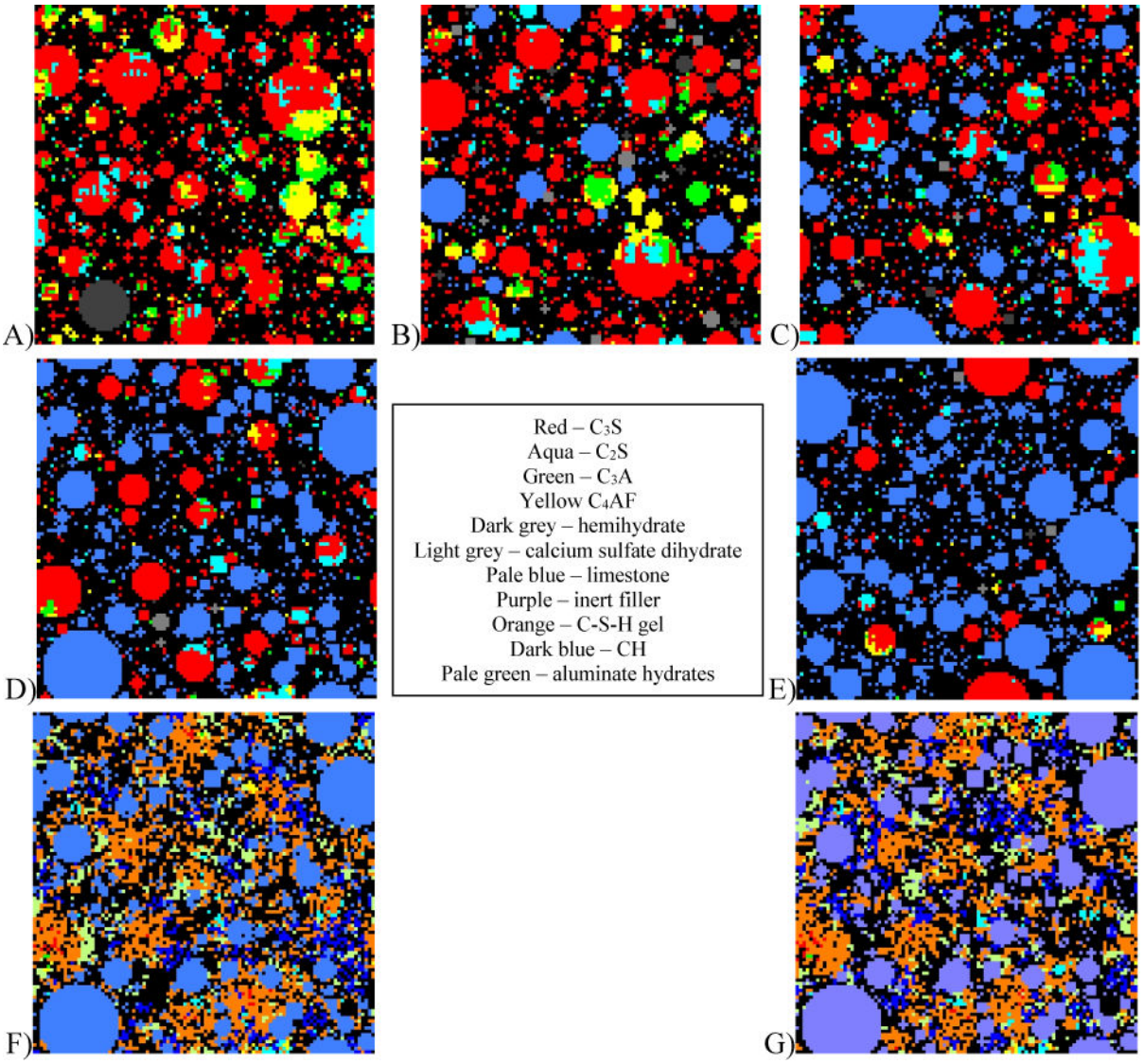


**Figure 2.**

2-D slice images (100 μm by 100 μm) from 3-D starting microstructures for hydration simulations for initial microstructures for: A) 100 % OPC, B) 20 % LS, C) 40 % LS, D) 60 % LS, and E) 80 % LS and hydrated microstructures (1000 cycles or 420 h) for F) 60 % LS and G) 60 % inert powder.[1]

[1]For the model phase identification, conventional cement chemistry notation is employed: C=CaO, S=$SiO_2$, A=$Al_2O_3$, F=$Fe_2O_3$, and H=$H_2O$

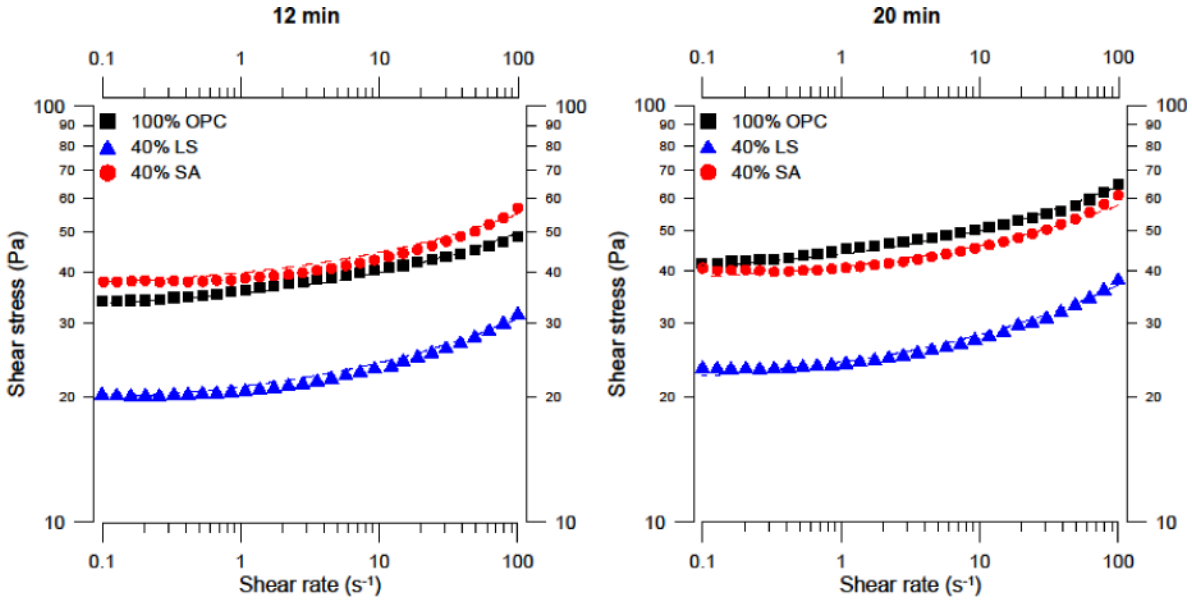


**Figure 3.**

Shear stress versus shear rate at 12 (left) and 20 min (right) hydration. The points correspond to the measured data and the line to the Herschel-Bulkley fittings. The uncertainty of the shear stress measurement could be estimated from the SRM 2492 certificate as about 6 % of the measured values [27].

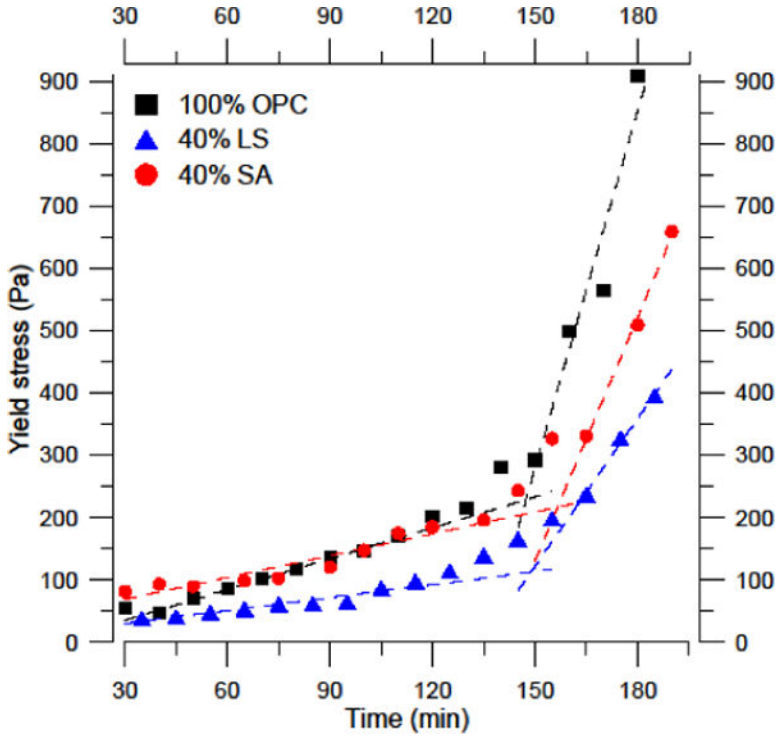


**Figure 4.**

Yield stress versus time during the first 3 h of hydration. Separate linear fits of the initial and after initial modification stages of the rheological properties are shown as dashed lines. The uncertainty of the yield stress measurement could be estimated from the SRM 2492 certificate as about 6 % of the measured value [27].

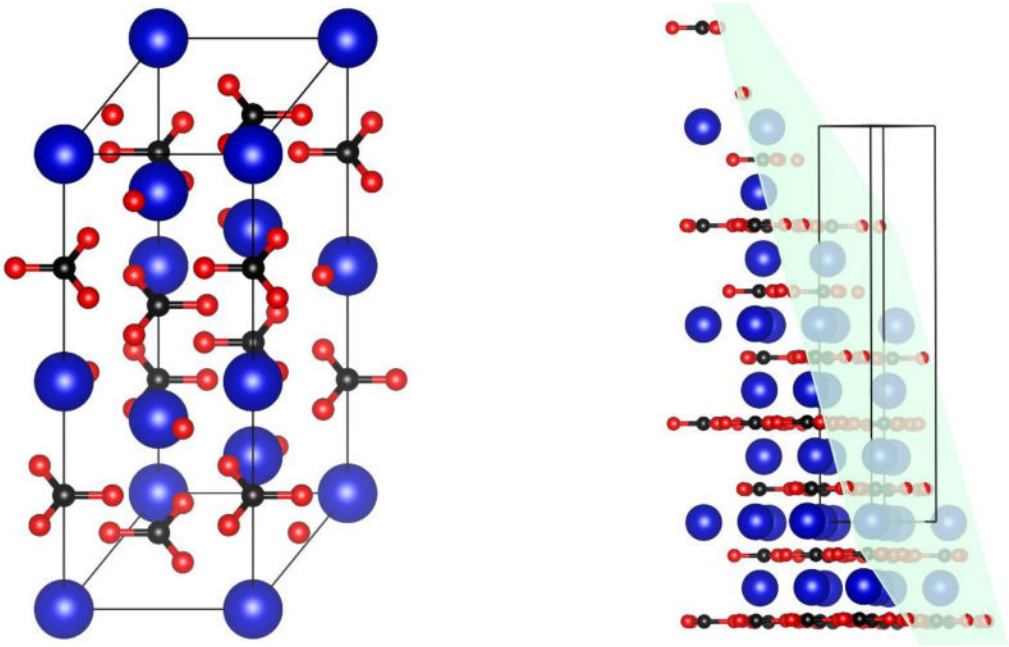

**Figure 5.**

Calcite unit cell general view (left) and dissected by $(10\bar{1}4)$ plane (right). Atom radius is reduced from actual values to allow better visualization. (Ca: large blue atoms; C: small black atoms; O: small red atoms, diagrams created using VESTA [34]).

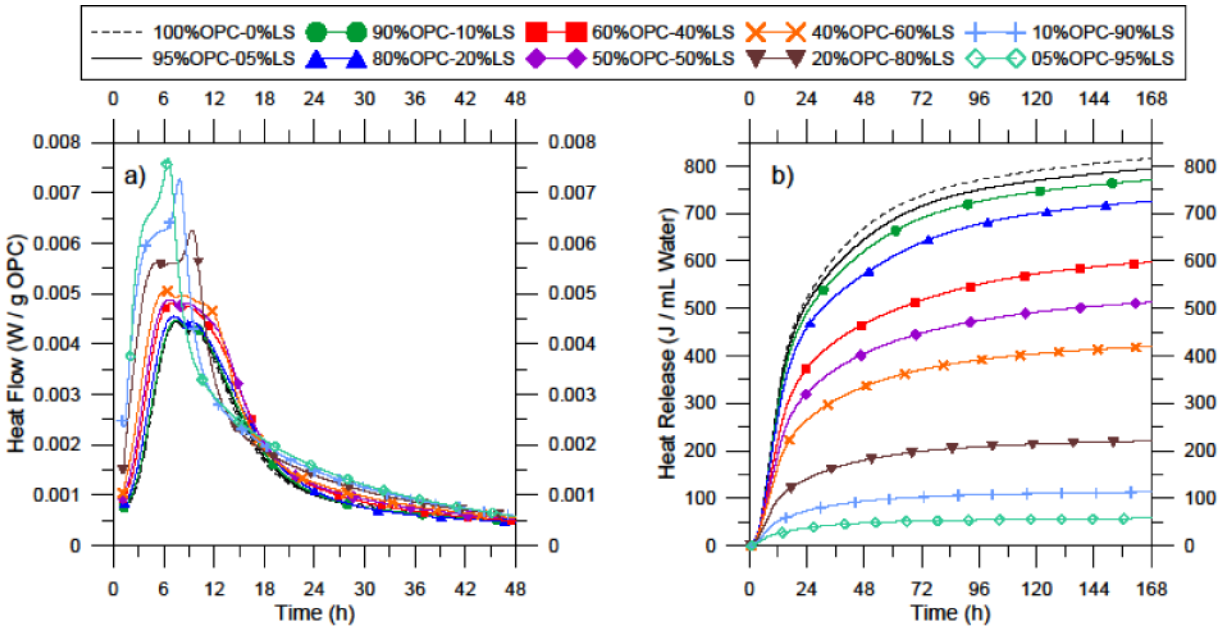


**Figure 6.**

Isothermal calorimetry results for paste mixtures with LS: a) heat flow normalized by mass of OPC and b) cumulative heat release plot normalized by initial volume of water.

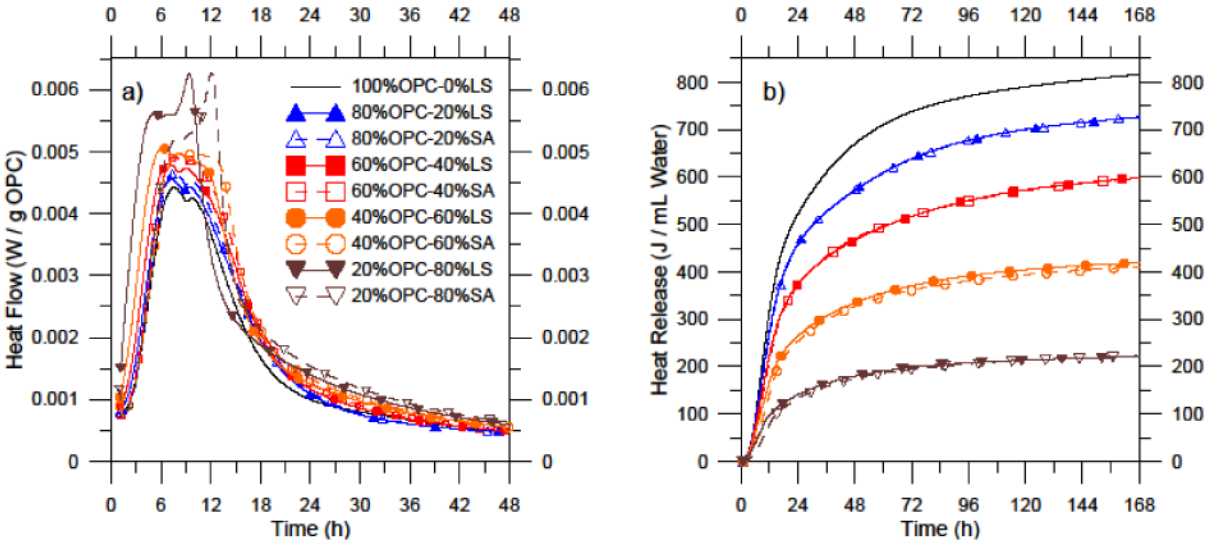


**Figure 7.**

Isothermal calorimetry results for paste mixtures with SA: a) heat flow normalized by mass of OPC and b) cumulative heat release plot normalized by initial volume of water.

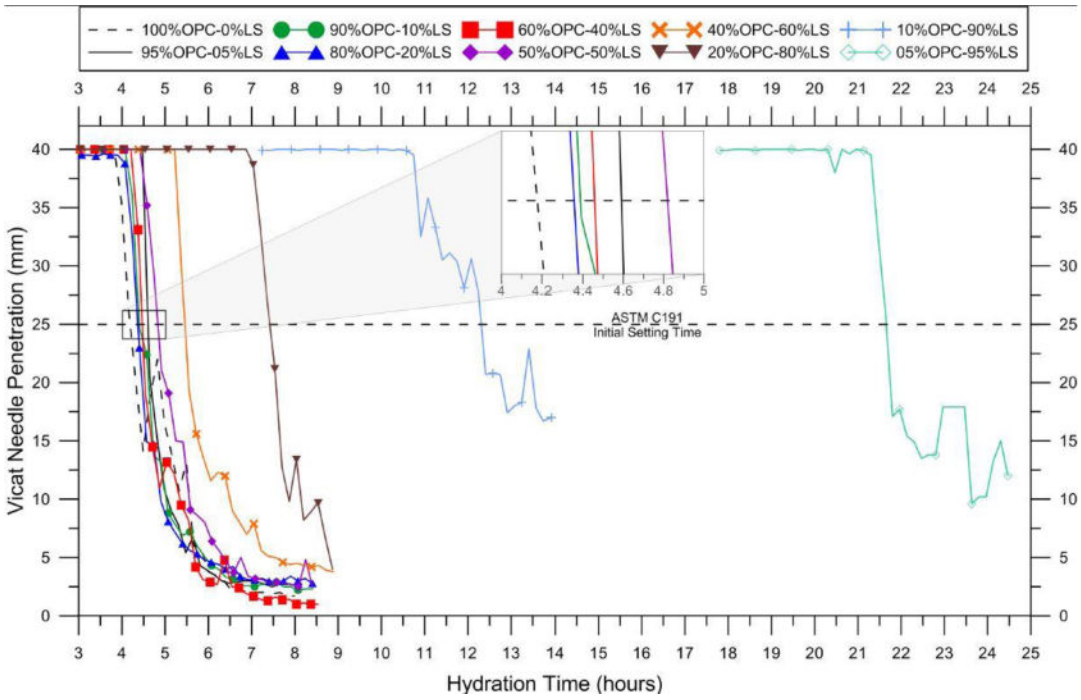


**Figure 8.**

Setting time results of paste mixtures with LS replacement as measured by ASTM C191 [25]. Below 40 % OPC-by-LS replacement, the additional surface effect of limestone dominates, while at 50 % and over, the dilution of cement offsets this enhancement, increasing setting times accordingly.

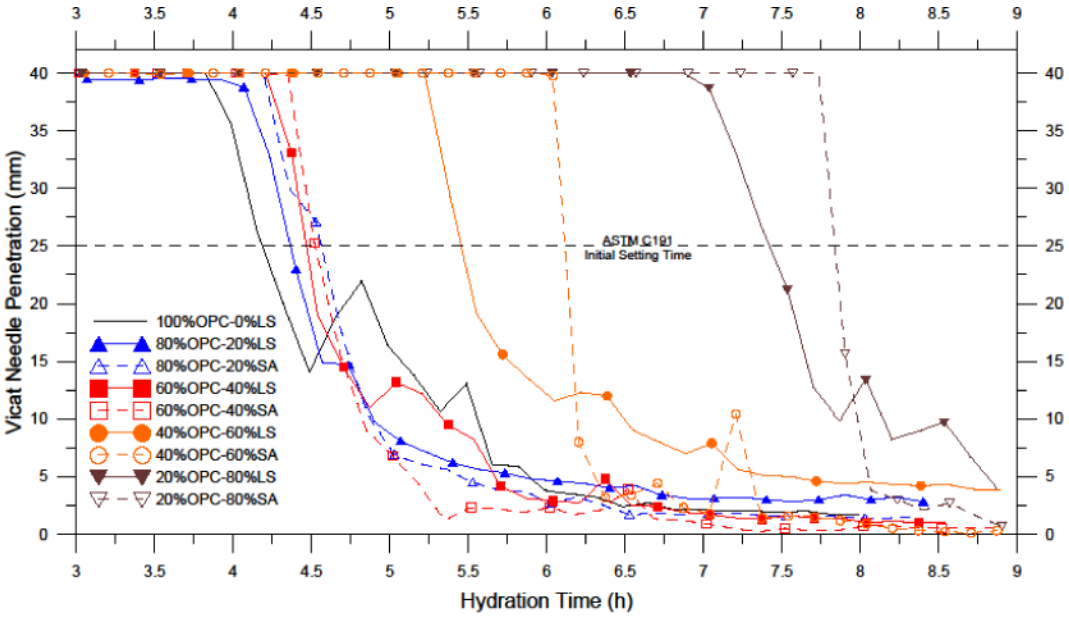


**Figure 9.**

Setting time results of paste mixtures with SA replacement as measured by ASTM C191 [25] in comparison to those with LS.

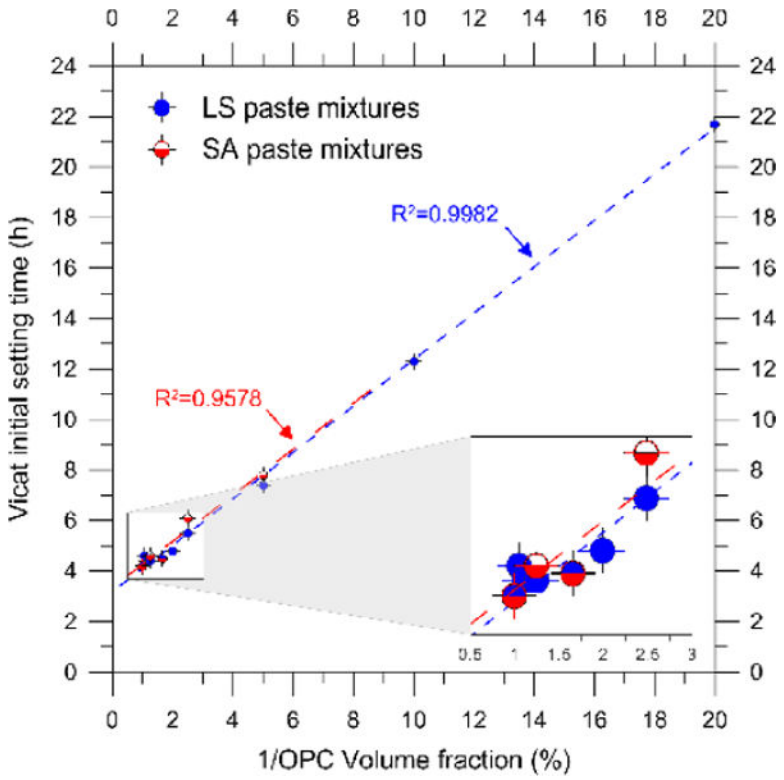


**Figure 10.**

Setting time results (ASTM C191 [25]) vs. OPC volume fraction of LS and SA mixtures showing a strong linear correlation, but with a relatively constant response (inset) for the higher OPC volume fractions (> 50 %).

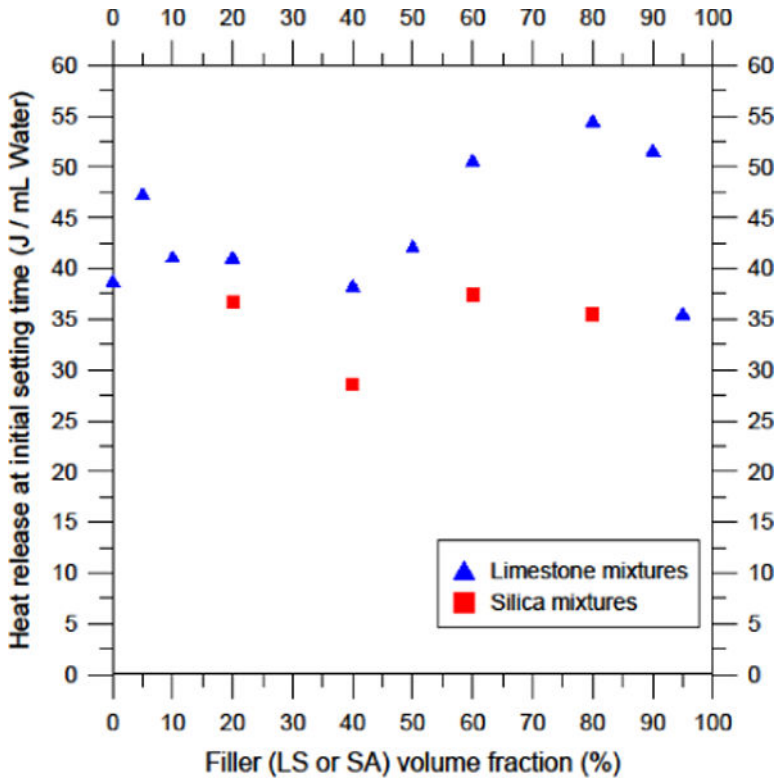


**Figure 11.**
Cumulative heat release achieved at initial time of set vs. filler content for the pastes.

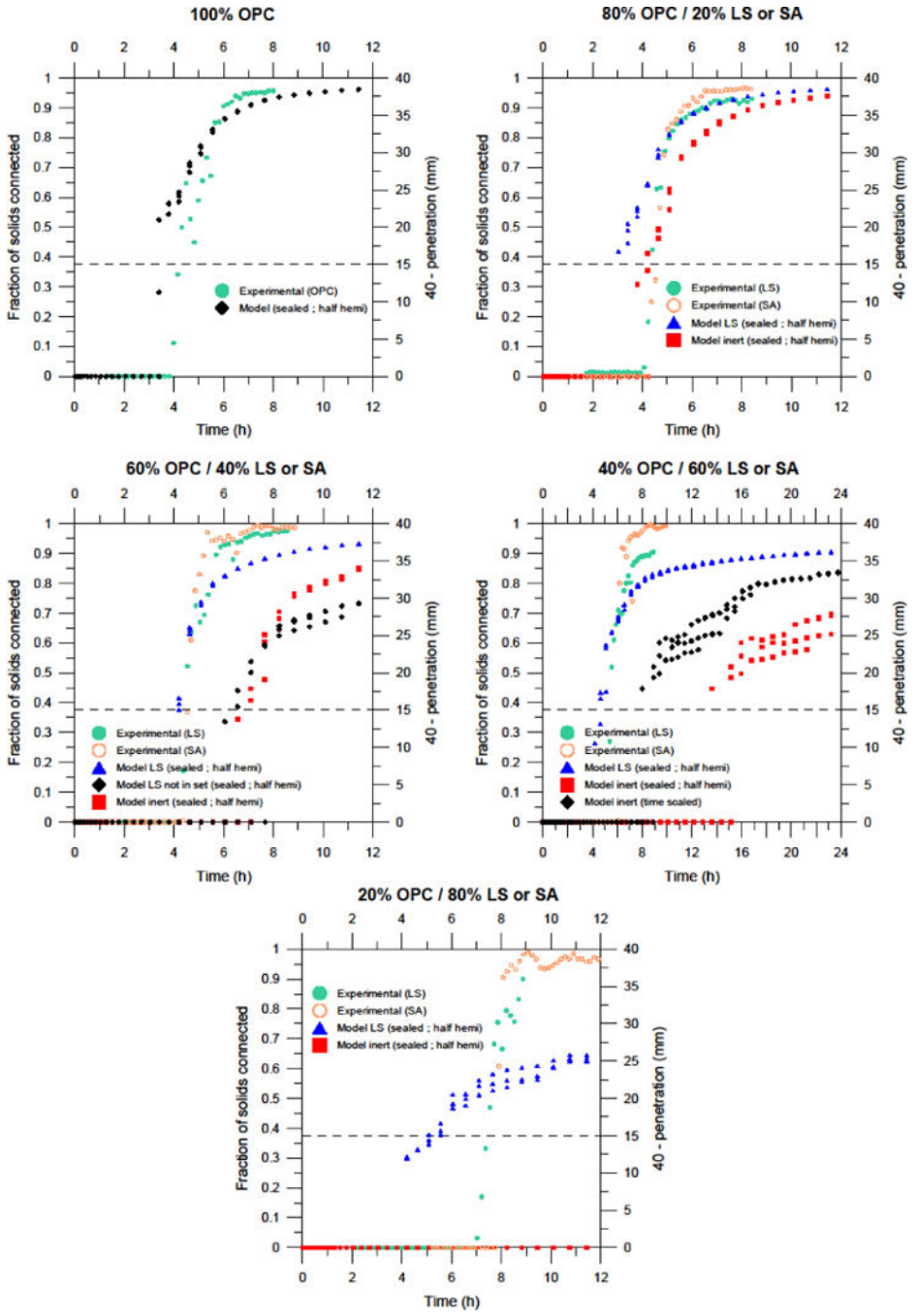


**Figure 12.**

Experimental Vicat needle penetration and simulated solids percolation (inert and limestone filler) results for five of the cement/limestone powder blended pastes investigated in the present study. 60:40 results include those for the case where limestone accelerates hydration, but limestone particles are not considered as part of the percolated backbone. 40:60 results indicate setting predictions for both original and time scaled (to better match experimental cumulative heat release curve) inert filler systems. Dashed line indicates penetration level corresponding to initial setting time.

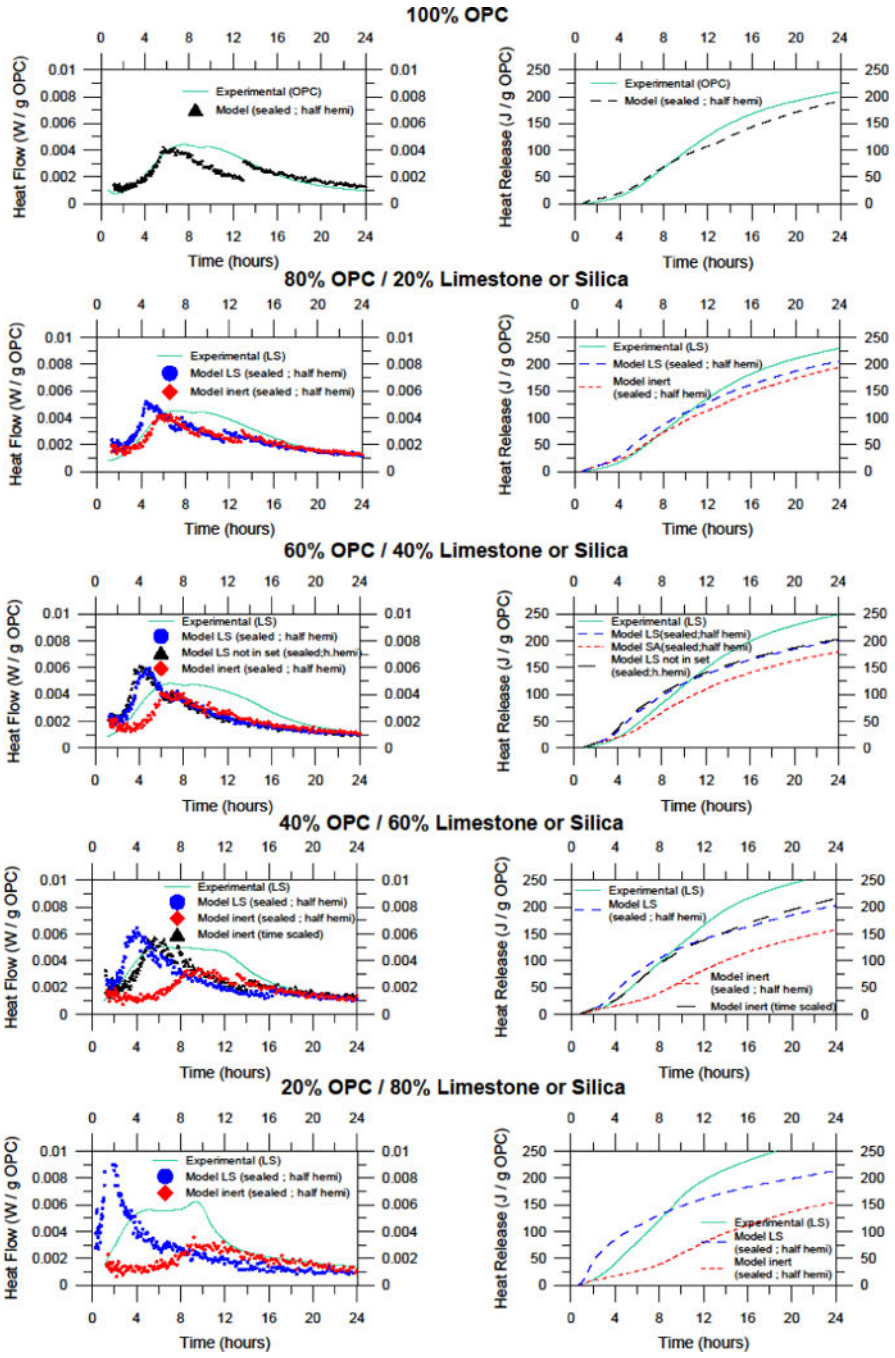


**Figure 13.**

Experimental and simulation (inert and limestone fillers) results for heat flow (left) and cumulative heat release (right) for five of the cement/limestone powder blended pastes investigated in the present study. 60:40 results include those for the case where limestone accelerates hydration, but limestone particles are not considered as part of the percolated backbone. 40:60 results indicate setting predictions for both original and time scaled (to better match experimental cumulative heat release curve) inert filler systems.

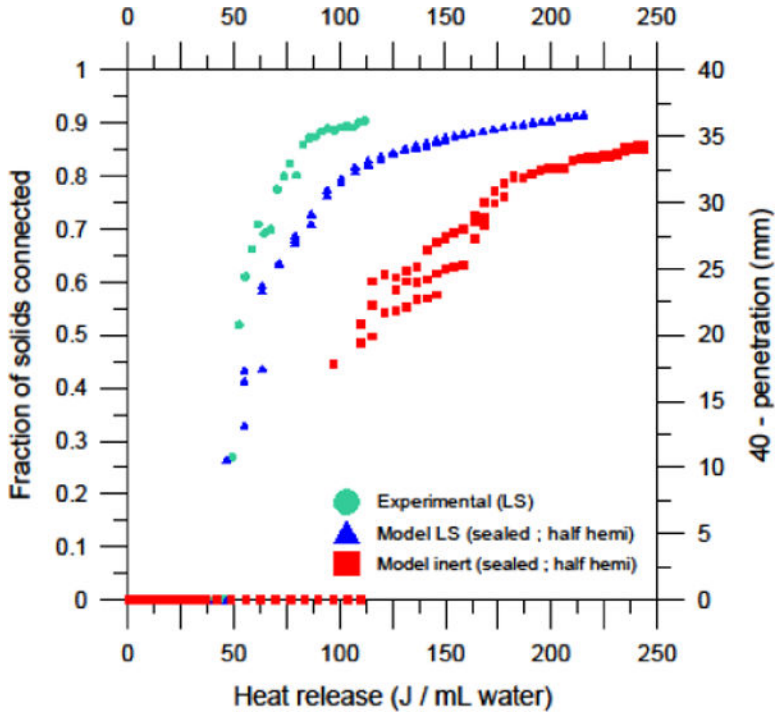


**Figure 14.**

Comparison of experimental and model setting vs. heat release results for 40:60 OPC:LS mixture.

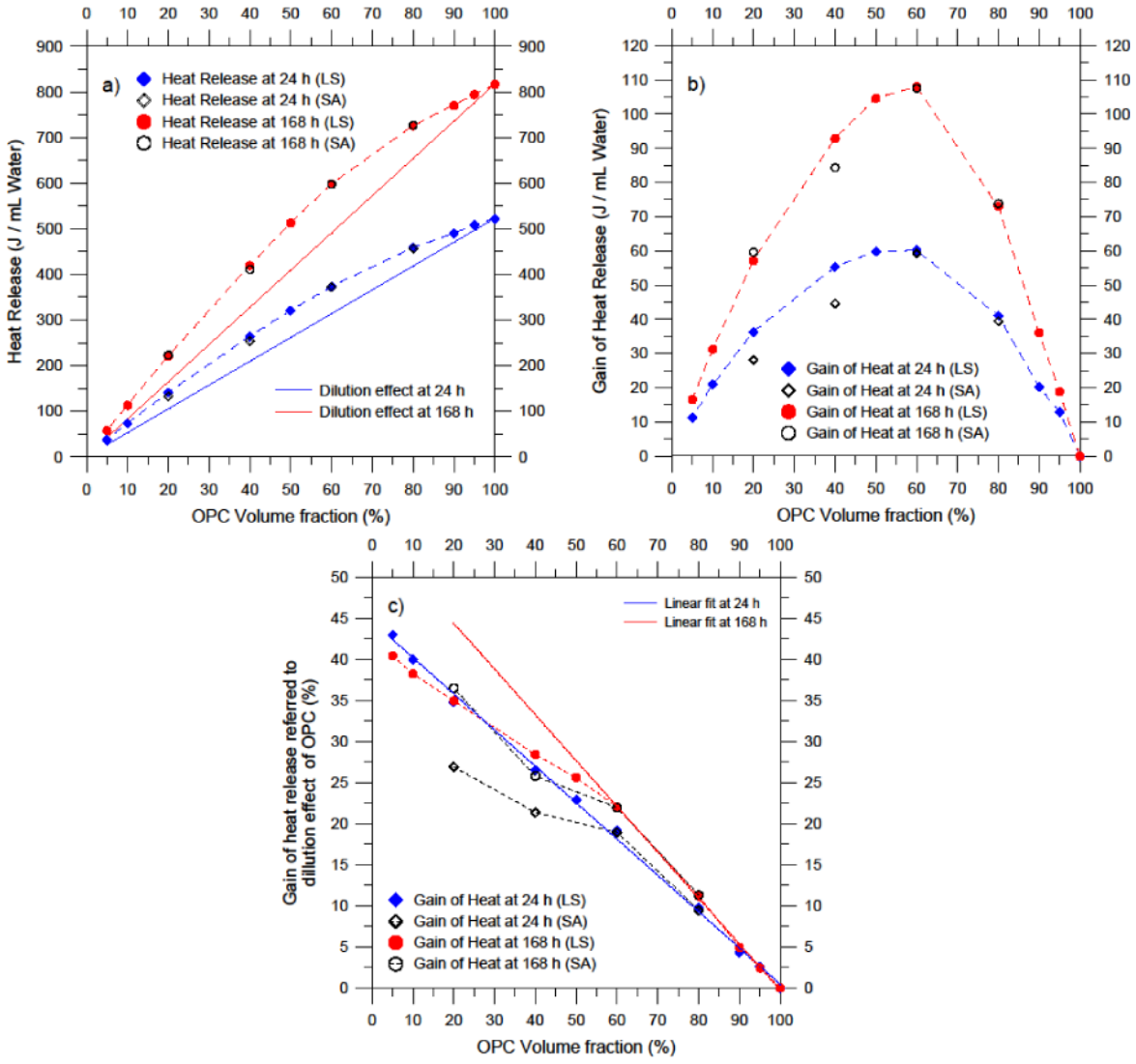


**Figure 15.**

Heat release (a) and gain in heat release (b) vs. OPC volume fractions for the LS and SA pastes prepared in the first study. (c) shows the heat gain referred to the potential heat release of the diluted OPC. Dashed lines between LS experimental results are provided as a visual guide.

**Table 1**

Characterization of raw materials.

| | OPC | Limestone | Silica |
|---|---|---|---|
| $SiO_2$ | 19.8 | – | 99.5 |
| $Al_2O_3$ | 4.81 | – | 0.30 |
| $Fe_2O_3$ | 3.14 | – | 0.02 |
| CaO | 63.4 | – | 0.02 |
| MgO | 2.75 | – | 0.01 |
| $SO_3$ | 2.91 | – | 0.00 |
| LOI | 2.71 | – | 0.20 |
| Total a1ka1ies[a] | 0.54 | – | 0.02 |
| $C_3S$ | 58.9 | – | – |
| $C_2S$ | 11.6 | – | – |
| $C_3A$ | 7.38 | – | – |
| $C_4AF$ | 9.46 | – | – |
| BET surface area ($m^2/g$) | 1.61 | 1.54 | 1.91 |
| Density ($kg/m^3$) | 3160 | 2740 | 2660 |
| BET surface area ($m^2/cm^3$) | 5.09 | 4.22 | 5.07 |

[a] $Na_2O + 0.658K_2O$

**Table 2**

Mixture proportions of cement pastes with OPC-by-LS or OPC-by-SA volume replacements.

| MIX ID | LS1 | LS2 | LS3 | LS4 | LS5 | LS6 | LS7 | LS8 | LS9 | LS10 | SA1 | SA2 | SA3 | SA4 |
|---|---|---|---|---|---|---|---|---|---|---|---|---|---|---|
| OPC (% vol. of solids) | 100 | 95 | 90 | 80 | 60 | 50 | 40 | 20 | 10 | 5 | 80 | 60 | 40 | 20 |
| Limestone powder (% vol. of solids) | 0 | 5 | 10 | 20 | 40 | 50 | 60 | 80 | 90 | 95 | – | – | – | – |
| Silica powder (% vol. of solids) | – | – | – | – | – | – | – | – | – | – | 20 | 40 | 60 | 80 |
| OPC (% mass of solids) | 100 | 95.6 | 91.2 | 82.2 | 63.4 | 53.6 | 43.5 | 22.4 | 11.4 | 5.7 | 82.7 | 64.1 | 44.3 | 23.0 |
| OPC (g) | 400 | 380 | 360 | 320 | 240 | 200 | 160 | 80 | 40 | 20 | 320 | 240 | 180 | 80 |
| Limestone powder (g) | 0 | 17.3 | 34.7 | 69.4 | 138.7 | 173.4 | 208.1 | 277.5 | 312.2 | 329.5 | – | – | – | – |
| Silica powder (g) | – | – | – | – | – | – | – | – | – | – | 67.1 | 134.2 | 201.3 | 268.4 |
| Water (g) | 160 | 160 | 160 | 160 | 160 | 160 | 160 | 160 | 160 | 160 | 160 | 160 | 160 | 160 |
| *w/p* ratio (by vol.) | 1.26 | 1.26 | 1.26 | 1.26 | 1.26 | 1.26 | 1.26 | 1.26 | 1.26 | 1.26 | 1.26 | 1.26 | 1.26 | 1.26 |
| *w/p* ratio (by mass) | 0.40 | 0.40 | 0.41 | 0.41 | 0.42 | 0.43 | 0.43 | 0.45 | 0.45 | 0.46 | 0.41 | 0.43 | 0.44 | 0.46 |

**Table 3**

Fitting parameters of the Herschel-Bulkley equation for the different mixtures at different times, using a spiral geometry. The uncertainty was not measured here, but can be estimated from the SRM 2492 certificate as ± 1.7 Pa for the yield stress and ± 0.74 Pa·s$^{-0.35}$ for the consistency factor [27].

| | **OPC 12 min** | **OPC 20 min** | **40 % Limestone 12 min** | **40 % Limestone 20 min** | **40 % Silica 12 min** | **40 % Silica 20 min** |
|---|---|---|---|---|---|---|
| $\tau_0$ (Pa) | 32 | 39 | 19 | 21 | 36 | 37 |
| $\mu$ (Pa·s$^{-0.35}$) | 3.5 | 5 | 2.4 | 3.2 | 3.8 | 4.1 |
| $n$ | 0.35 | 0.35 | 0.35 | 0.35 | 0.35 | 0.35 |